# Actuator Fault Diagnosis and Control of a Quadrotor

Adilson de Souza Cândido*, Roberto Kawakami Harrop Galvão† and Takashi Yoneyama‡
Department of Electronic and Computer Engineering
Instituto Tecnológico de Aeronáutica – ITA, São José dos Campos, SP, Brazil
Emails: candido@ita.br*, kawakami@ita.br† and takashi@ita.br‡

***Abstract*—This paper addresses the problem of actuator fault diagnosis and control of a realistic nonlinear six degree-of-freedom quadrotor helicopter model, based on interacting multiple model (IMM) filter and a switching multi-model predictive controller (MMPC). The proposed methods were evaluated by numerical simulation, and the faults were modeled by increasing the friction and temperature of one rotor. The results were satisfactory in terms of fault detection and diagnosis while performing accurate reference tracking.**

***Keywords*—Unmanned quadrotor helicopter; interacting multiple model filter; fault diagnosis; multi-model predictive controller; actuator fault and brushless dc motor.**

## I. Introduction

Quadrotor helicopters have become increasingly popular, with various civil and military applications, due to their simple construction, accurate low-speed maneuver and hovering capabilities [1].

In order to ensure the normal operation, and increase the safety, reliability and mission dependability of such vehicles, the problem of fault detection and diagnosis is very important. Several methods have been developed to fault detection and diagnosis of quadrotors [2]. However only few researches have been devoted to the important problem of detecting the vehicle actuator faults [3]. The solution proposed in this paper permits to detect and isolate which rotor is faulty, measuring only few accessible signals most commonly used in Electronic Speed Controllers (ESC) for Brushless DC Motors: motor armature current [4] and rotor position feedback [5]. The solution is based on the Interacting Multiple Model (IMM) filter, which has been shown to be one of the most cost-effective adaptive estimation techniques for systems involving structural as well as parametric changes [6].

Another critical issue is to design an efficient controller for a non-linear and sub-actuated quadrotor, subject to system constraints, in a variety of flight conditions and faults. Some proposed solutions involve the use of Proportional-Integral-Derivative controller (PID controller), Linear Quadratic Regulator (LQR), backstepping and sliding-mode controllers [1]. Here, a cascade switching multi-model predictive controller based on a piecewise affine (PWA) linear model of the quadrotor's dynamics is adopted. The satisfactory performance of the Model Predictive Controller (MPC) and its inherent degree of fault tolerance was already demonstrated in [7].

The overall structure of this paper is given as follows. Section II briefly introduces the models for the quadrotor that comprise the brushless DC motor. Section III presents the design of the switching multi-model predictive controller for the quadrotor's tracking control problem. In Section IV we have compiled some basic facts about the adopted fault diagnosis approach. Finally, Section V presents some numerical simulation results followed by concluding remarks in the last Section.

## II. Quadrotor Model

The model of the quadrotor used in this work assumes that the structure is rigid and symmetrical, the center of gravity and the origin of the body fixed frame coincide, according to Figure 1, the thrust and drag forces are proportional to the square of propeller's angular velocity $\Omega_i$ for $i = 1, \ldots, 4$, and the propellers are rigid.

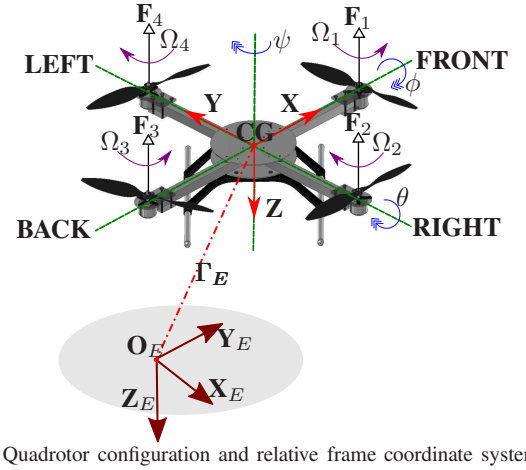


Fig. 1. Quadrotor configuration and relative frame coordinate systems

The dynamic model of the quadrotor can be obtained by the Newton-Euler formalism and is described by the following state space equation of motion [8]:

$$\begin{bmatrix} \dot{\phi} \\ \ddot{\phi} \\ \dot{\theta} \\ \ddot{\theta} \\ \dot{\psi} \\ \ddot{\psi} \\ \dot{Z} \\ \ddot{Z} \\ \dot{X} \\ \ddot{X} \\ \dot{Y} \\ \ddot{Y} \end{bmatrix} = \begin{bmatrix} \dot{\phi} \\ \dot{\theta}\dot{\psi}\left(\frac{I_{YY}-I_{ZZ}}{I_{XX}}\right)+\dot{\theta}\frac{J_{TP}}{I_{XX}}\Omega+\frac{1}{I_{XX}}U_2 \\ \dot{\theta} \\ \dot{\phi}\dot{\psi}\left(\frac{I_{ZZ}-I_{XX}}{I_{YY}}\right)-\dot{\phi}\frac{J_{TP}}{I_{YY}}\Omega+\frac{1}{I_{YY}}U_3 \\ \dot{\psi} \\ \dot{\theta}\dot{\phi}\left(\frac{I_{XX}-I_{YY}}{I_{ZZ}}\right)+\frac{1}{I_{ZZ}}U_4 \\ \dot{Z} \\ g-(\cos\phi\cos\theta)\,U_1/m \\ \dot{X} \\ (\cos\phi\sin\theta\cos\psi+\sin\phi\sin\psi)\,U_1/m \\ \dot{Y} \\ (\cos\phi\sin\theta\sin\psi-\sin\phi\cos\psi)\,U_1/m \end{bmatrix} + \begin{bmatrix} 0 \\ \tilde{W}_1 \\ 0 \\ \tilde{W}_2 \\ 0 \\ \tilde{W}_3 \\ 0 \\ \tilde{W}_4 \\ 0 \\ \tilde{W}_5 \\ 0 \\ \tilde{W}_6 \end{bmatrix} \quad (1)$$

where $I_{XX}$, $I_{YY}$ and $I_{ZZ}$ are respectively X-axis, Y-axis and Z-axis inertia components, $\mathbf{\Gamma_E} = [X\ Y\ Z]$ is the translation-vector movement of the quadrotor's center of mass, $[\phi\ \theta\ \psi]$ is respectively the roll, pitch and yaw angles, $\Omega$ is the overall residual propeller angular speed, $J_{TP}$ is the rotational moment of inertia around the propeller axis, $g$ is the acceleration due to gravity, and $\tilde{W}_i, i = 1, \ldots, 6$ corresponds to the effect of the unknown "additive" disturbance (such as a wind gust) on the system's dynamics [8].

The control input vector is defined by

$$\begin{bmatrix} U_1 \\ U_2 \\ U_3 \\ U_4 \\ \Omega \end{bmatrix} = \begin{bmatrix} b\left({\Omega_1}^2 + {\Omega_2}^2 + {\Omega_3}^2 + {\Omega_4}^2\right) \\ l\ b\left(-{\Omega_2}^2 + {\Omega_4}^2\right) \\ l\ b\left({\Omega_1}^2 - {\Omega_3}^2\right) \\ l\ d\left(-{\Omega_1}^2 + {\Omega_2}^2 - {\Omega_3}^2 + {\Omega_4}^2\right) \\ -\Omega_1 + \Omega_2 - \Omega_3 + \Omega_4 \end{bmatrix} \quad (2)$$

where $l$ is the quadrotor's arm length, $b$ is the thrust coefficient, $d$ is the drag coefficient, the input $U_1$ is related with the total thrust, and the inputs $U_2$, $U_3$ and $U_4$ are related with the roll, pitch and yaw rotations of the quadrotor, respectively.

### A. Brushless DC electric motor

Most of the quadrotors use brushless DC electric motors, mainly because of their low cost and high power density allied to low weight [1]. A general representation of the actuator and the electronic speed controller (ESC) can be seen in Figure 2.

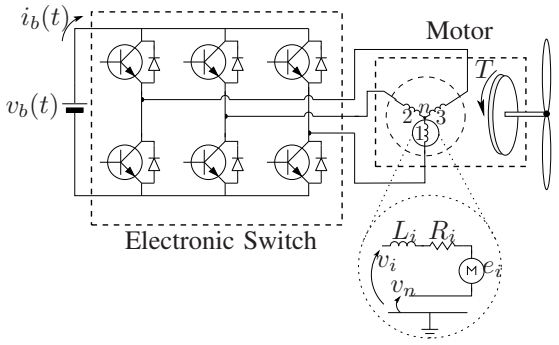


Fig. 2. General representation of each actuator of the quadrotor driven by a brushless DC electric motor

It can be shown [9] that the model of the electronically commutated brushless DC motor is similar to the model of the classical DC motor, described by

$$\begin{cases} \bar{v}(t) = R\ \bar{i}(t) + K_M\ \omega_M(t) \\ \dot{\omega}_M = \dfrac{K_M}{J_{TP}}\bar{i} - \dfrac{d}{J_{TP}}[\omega_M]^2 - \dfrac{c_c}{J_{TP}}\text{sign}[\omega_M] - \dfrac{c_v}{J_{TP}}\omega_M \end{cases} \quad (3)$$

where $\bar{v}(t)$ $[V]$ and $\bar{i}(t)$ $[A]$ are the average phase voltage and current respectively, $R = 2/3(R_1 + R_2 + R_3)$ $[\Omega]$ is the equivalent electric resistance derived from the Joule loss of each coil, $K_M = 2/3(K_{M1} + K_{M2} + K_{M3})$ $[V\,s/rad]$ is the back electromotive force (emf) constant (considered equal to the torque constant), $\omega_M$ $[rad/s]$ is the angular velocity, $c_c$ $[N\,m]$ and $c_v$ $[N\,m\,s/rad]$ are respectively the Coulomb (static) and viscous (dynamic) friction coefficients.

Based on (3), it is possible to describe a general set $\mathbb{S}$ of nonlinear discrete-time systems models, each of which closely related to a specific condition, as

$$S_j : \begin{cases} x(k+1) = f\left[x(k), u(k), k\right] + q(k) \\ y(k) \quad\ = h\left[x(k), u(k), k\right] + r(k) \end{cases}, \forall S_j \in \mathbb{S} \quad (4)$$

where we assume both the process and measurement noises are additive, $q(k) \sim \mathcal{N}\big[0, Q(k)\big]$, $r(k) \sim \mathcal{N}\big[0, R(k)\big]$, $x(k) \in \mathbb{R}^n$ is the state of the system at time step $k$, $y(k) \in \mathbb{R}^m$ is the measurements vector, and $u(k) \in \mathbb{R}^{l_u}$ is the input vector.

## III. Switching Multi-Model Predictive Control

The main idea in Model-based Predictive Control (MPC) is to use the mathematical description of the system to be controlled (model), in order to predict its future state corresponding to a class of inputs and choose the best one, according to a performance index. MPCs have the advantage of allowing constraints of the systems parameters in an explicit form [10]. It had already been successfully used in other areas including chemical, food processing, automotive, and aerospace applications [8], [10] and [11].

Switching multi-model predictive controller is an effective manner for fault accommodation and system stabilization [12], even in the presence of large flight envelope [13]. It is based on an effective switching among a bank of model predictive controllers, each designed considering local models.

According to the Figure 3, the MPC is composed by:

- *Multi-Model Structure*: A model of the plant that is used to predict the state of the plant $\widehat{x}(k+i|k)$ from the discrete time index $k$ to $i$ steps into the future with $i = 1, \ldots, N$, where $N$ is the prediction horizon. These predictions are based on the current state $x(k)$ and the predicted control sequence $\widehat{u}(k+i-1|k)$, previously estimated over the horizon $i = 1, \ldots, M$. In this paper, this model is former by a collect of piecewise linear affine (PWA) models of (1), and the aerodynamic forces are considered like external disturbances for the control design purposes.
- *Optimizer*: The optimizer calculates the best control sequence that minimize a cost function and respect possible constraints on inputs and states of the plant. However, only the first of this sequence, $\widehat{u}^*(k|k)$, is actually applied to the plant at each sample time.

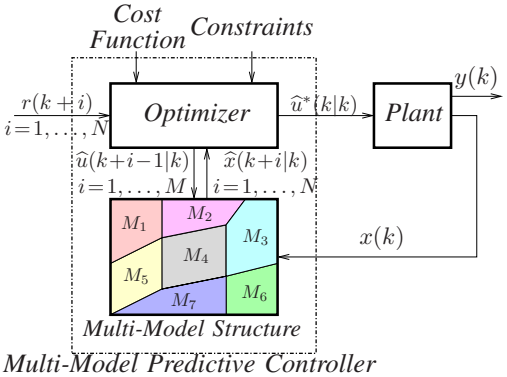


Fig. 3. Switching multi-model predictive controller with state feedback

The $i$th model in the model set $\mathbb{M} = M_1, M_2, \ldots, M_{MS}$ can be described by

$$M_i : \begin{cases} x(k+1) &= A_i(k)\ x(k) + B_i(k)\ u(k) \\ y(k) &= C_i(k)\ x(k) \end{cases} \quad (5)$$

where the matrices $A_i(k)$, $B_i(k)$ and $C_i(k)$ may all be different for different $i = 1, \ldots, MS$. The switching among the models $\forall M_i \in \mathbb{M}$ are commanded by a supervisor module, based, for instance, on the distance between the actual system state and the linearization points of the PWA models.

The cost function used in this work is the usual one:

$$\mathbb{J} = \sum_{i=1}^{N} \|\widehat{y}(k+i|k) - r(k+i)\|^2_{\boldsymbol{\gamma}} + \sum_{i=1}^{M} \|\widehat{u}(k+i-1|k)\|^2_{\boldsymbol{\rho}} + \sum_{i=1}^{N} \|\widehat{z}(k+i|k)\|^2_{\boldsymbol{\mu}} \quad (6)$$

where $\boldsymbol{\gamma}$, $\boldsymbol{\rho}$ and $\boldsymbol{\mu}$ are the matrix cost weight, $M$ is the control horizon, $N$ is the prediction horizon, and $\widehat{z}(k+i|k) = \widehat{z}(k+i-1) + r(k+i) - \widehat{y}(k+i|k)$ is the accumulated error, used to provide integral action for the controller.

In addition, the constraints are

$$\begin{cases} U_{min} \leq \widehat{u}(k-1+i|k) \leq U_{max} & i = 1, \ldots, M \\ \Delta U_{min} \leq \Delta\widehat{u}(k-1+i|k) \leq \Delta U_{max} & i = 1, \ldots, M \\ Y_{min} \leq \widehat{y}(k+j|k) \leq Y_{max} & j = 1, \ldots, N \end{cases}$$

and it can be shown that this optimization problem is reduced to the solution of a quadratic function [14].

### A. Cascade model predictive control for the quadrotor

The quadrotor is controlled with three cascade predictive controllers, as depicted in Figure 4, for the control of the altitude ($Z$), position ($X$ and $Y$) and attitude ($\phi$, $\theta$ and $\psi$) of the unmanned aerial vehicle.

According to Figure 4, the innermost control loop is the attitude control, which receives the yaw reference from the guidance system and the references of roll and pitch from the position control loop. Based on these references and the state vector $[\phi\ \dot{\phi}\ \theta\ \dot{\theta}\ \psi\ \dot{\psi}]^T$ the MPC calculates the control signal $[U_2\ U_3\ U_4\ \Omega]^T$. The next control loop is the position control that calculates the necessary angular reaction $[\phi_R\ \theta_R]^T$, based on the state vector $[X\ \dot{X}\ Y\ \dot{Y}]^T$, the thrust force $U_1$, and the references from the guidance system related to the quadrotor desired position $[X_R\ Y_R]^T$. The last control loop calculates the total thrust necessary to provide the desired elevation specified by the guidance system, according to the state vector $[Z\ \dot{Z}]^T$.

Each of these controllers use a set of discrete piecewise linear affine model of the non-linear dynamic (1). The active region (or active mode) $j_i$ of the PWA system is selected at each sample time by evaluating (7) for the current value of the state $\boldsymbol{x}_i$.

$$S_i = \arg\min_{j_i} \|\boldsymbol{x}_i - \boldsymbol{x}^{\circ}_{i,j_i}\| \quad (7)$$

where the index $i = \{AL;\ PC;\ AT\}$ is related to the process control loops (altitude control $AL$, position control $PC$, and attitude control $AT$), the index $j_i = \{1, 2, \cdots, s_i\}$ denotes the number of affine subsystems, and $\boldsymbol{x}^{\circ}_{i,j_i}$ is the respective linearization points.

## IV. Fault Detection and Diagnosis

During a long time mission it is very probable that one of rotors of a quadrotor becomes faulty and partially loses its effectiveness [15]. If one uses a tool to detect this fault then it might be possible to choose a strategy to overcome this faulty condition and at least land the quadrotor safely [15].

The Interacting Multiple Model (IMM) is promising for Fault Detection and Diagnosis (FDD) because, among others [6], it is possible to estimate the information of the type of fault (sensor or actuator), location (which sensor or actuator), size (total or partial failures) and fault occurrence time. Moreover, for partial faults, the magnitude can be estimated by the probabilistically weighted sum (a convex combination) of the system models [6].

The IMM filter is depicted in Figure 5 which represents the four major steps that must be solved at each cycle [6]: interaction, filtering (bank of filters), model probabilities update and combination.

As described in Figure 5, the first block, "Interaction", consists on the re-initialization of the bank of filters by mixing all the estimates at the previous time. The second block, "Bank

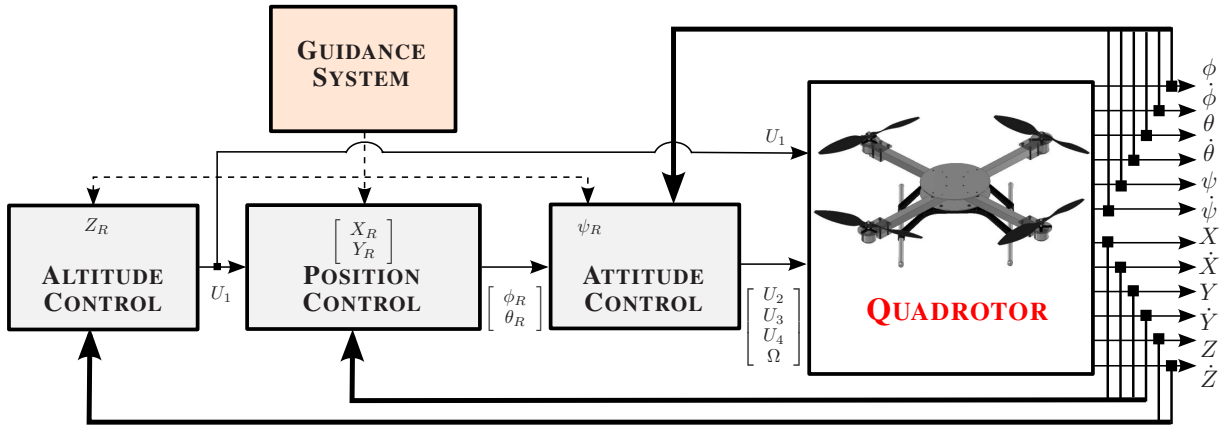


Fig. 4. Quadrotor switching multi-model predictive controller with state feedback

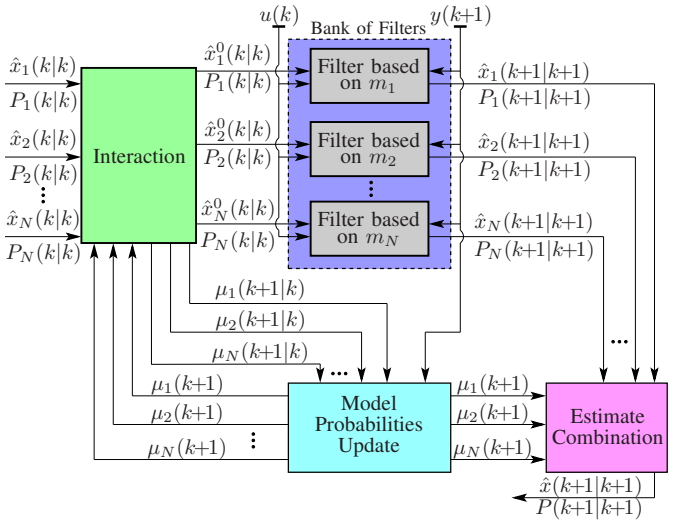


Fig. 5. Basic representation of the IMM algorithm

of Filters", consists of a set of model-conditional filters that provide the state estimation based on a set of local models. The third block, "Model Probabilities Update", estimates the probability that each model describes the current dynamic. Finally, the last block evaluate the overall state estimation. Table I presents a summary of the IMM algorithm cycle [6] that use a bank of Unscented Kalman Filters (UKF), based on the set of non-linear motor model (4).

A detailed description of the UKF algorithm can be found in [16], but the basic idea is to choose a minimal set of sample points (called sigma points) around the mean. These sigma points are then propagated through the non-linear functions, from which the mean and covariance of the estimate are then recovered. These estimations are incorporated efficiently into the IMM algorithm to perform effective fault detection (no false alarms or missed faults), based on a fault detection threshold.

In [6] an universal fault detection threshold $\mu_T$ was proposed, so that

$$\text{If } \bar{\mu}_j(k+1) = \max_j \mu_j(k+1) \begin{cases} < \mu_T & \text{no fault} \\ > \mu_T & \text{fault } j \text{ occurred} \end{cases} \tag{8}$$

However, this strategy could cause false detection alarms, especially on transient response or for small parameters drift changes, since it considers only the actual probability $\mu_j(k+1)$ at each period of time. In order to balance false alarms against missed detection, is proposed in this work the index $I_j(k)$ for all the models $j = 1, \ldots, N$, as described by equation

$$I_j(k) = \alpha_j \mu_j(k) + \beta_j \sum_{i=k-1}^{k-1-H_0} \lambda_j^{k-1-i} \mu_j(i) \tag{9}$$

where $\alpha_j \geq 0$, $\beta_j \geq 0$, and respectively $H_0$ and $\lambda_j \in [0, 1]$ are the memory width and depth (related to a "forgetting factor" which gives exponentially less weight to older probabilities).

The fault detection signal can be determined based on the performance index

$$S_j(k) = H\left[\Delta I_j(k)\right] \tag{10}$$

where $\Delta I_j(k) = I_j(k) - I_{max}(k)$, and $I_{max} = \max_j I_j$ for $j = 1, \ldots, N$, and $H[x]$ is the Heaviside unit step function. Therefore,

$$\text{If } S_j(k) \begin{cases} = 0 & \text{no fault} \\ = 1 & \text{possible fault related to } j\text{th model} \end{cases} \tag{11}$$

## V. Simulation Results

The proposed solution was validated by numerical simulations in order to evaluate the performance of the fault detection and diagnosis system, based on the Omnidirectional Stationary Flying OUtstretched Robot – OS4 Mini-VTOL [1], which the main design variables are listed in Table II. The motor is mounted to a gearbox with a reduction ratio of 4:1, and for online fault detection, built-in sensors were used to measure the supply voltage, current and rotor position.

Table I. One cycle of the Interacting Multiple Model (IMM)

| | |
|---|---|
| (1) *Mixing of the estimates* | (for j = 1,..., N) |
| Predicted mode probability: | $\mu_j(k+1\|k) \triangleq P(m_j(k+1)\|y(k)) = \sum_{i=1}^{N} \pi_{ij}\mu_i(k)$ |
| Mixing probability: | $\mu_{i\|j} \triangleq P(m_i(k)\|m_j(k+1), y(k)) = \pi_{ij}\mu_i(k)/\mu_j(k+1\|k)$ |
| Mixing estimate: | $\hat{x}_j^0(k\|k) \triangleq E[x(k)\|m_j(k+1), y(k)] = \sum_{i=1}^{N} \hat{x}_i(k\|k)\mu_{i\|j}(k)$ |
| Mixing covariance: | $P_j^0(k\|k) \triangleq cov[\hat{x}_j^0(k\|k)\|m_j(k+1), y(k)] = \sum_{i=1}^{N} \left\{P_i(k\|k) + \left[\hat{x}_j^0(k\|k) - \hat{x}_i(k\|k)\right]\left[\hat{x}_j^0(k\|k) - \hat{x}_i(k\|k)\right]^T\right\}\mu_{i\|j}(k)$ |
| (2) *Non-linear filtering* | (for j = 1,..., N and i=1,...,2n+1 weighted samples or sigma points) |
| Propagate each sigma point: | $\mathcal{X}_i(k+1\|k) = f\left[\mathcal{X}_i(k\|k), u(k), k\right]$ |
| Predicted state: | $\hat{x}_j(k+1\|k) \triangleq E[x(k+1\|m_j(k+1), y(k)] = \sum_{i=0}^{2n} W_i \mathcal{X}_i(k+1\|k)$ |
| Predicted covariance: | $P_j(k+1\|k) \triangleq cov[\hat{x}_j(k+1\|k)\|m_j(k+1), y(k)] = \sum_{i=0}^{2n} W_i\left\{\mathcal{X}_i(k+1\|k) - \hat{x}(k+1\|k)\right\}\left\{\mathcal{X}_i(k+1\|k) - \hat{x}(k+1\|k)\right\}^T$ |
| Updated state: | $\hat{x}_j(k+1\|k+1) \triangleq E[x(k+1)\|m_j(k+1), y(k+1)]$ |
| Updated covariance: | $P_j(k+1\|k+1) \triangleq cov[\hat{x}_j(k+1\|k+1)\|m_j(k+1), y(k+1)]$ |
| (3) *Model probability update* | (for j = 1,..., N) |
| Likelihood function: | $L_j(k+1) \triangleq \mathcal{N}[v_j(k+1), 0, S_j] = \frac{1}{\sqrt{\lvert 2\pi S_j\rvert}} exp\left[-\frac{1}{2} v_j^T S_j^{-1} v_j\right]$ |
| Mode probability: | $\mu_j(k+1) \triangleq P[m_j(k+1)\|y(k+1)] = \frac{\mu_j(k+1\|k)L_j(k+1)}{\sum_{i=1}^{N} \mu_i(k+1\|k)L_i(k+1)}$ |
| (4) *Combination of estimates* | |
| Overall state estimate: | $\hat{x}(k+1\|k+1) \triangleq E[x(k+1)\|y(k+1)] = \sum_{i=1}^{N} \hat{x}_i(k+1\|k+1)\mu_i(k+1)$ |
| Overall covariance: | $P(k+1\|k+1) \triangleq E\left[\left[x(k+1) - \hat{x}(k+1\|k+1)\right]\left[x(k+1) - \hat{x}(k+1\|k+1)\right]^T\|y(k+1)\right] =$ |
| | $= \sum_{i=1}^{N} \left\{P_i(k+1\|k+1) + \left[\hat{x}(k+1\|k+1) - \hat{x}_i(k+1\|k+1)\right] \cdot \left[\hat{x}(k+1\|k+1) - \hat{x}_i(k+1\|k+1)\right]^T\right\}\mu_i(k+1)$ |

Table II. OS4 PARAMETERS

| Symbol | Parameter | Value |
|---|---|---|
| $m$ | Overall Mass | $6{,}50 \times 10^{-1}\ [Kg]$ |
| $I_{XX}$ | Moment of inertia about the $x$-axis | $7{,}50 \times 10^{-3}\ [Kg\ m^2]$ |
| $I_{YY}$ | Moment of inertia about the $y$-axis | $7{,}50 \times 10^{-3}\ [Kg\ m^2]$ |
| $I_{ZZ}$ | Moment of inertia about the $z$-axis | $1{,}30 \times 10^{-2}\ [Kg\ m^2]$ |
| $b$ | Thrust Coefficient | $3{,}13 \times 10^{-5}\ [N\ s^2]$ |
| $d$ | Drag Coefficient | $7{,}5 \times 10^{-7}\ [N\ m\ s^2]$ |
| $l$ | Arm Length | $2{,}30 \times 10^{-1}\ [m]$ |
| $J_{TP}$ | Rotational Moment of Inertia | $5{,}60 \times 10^{-6}\ [Nms^2]$ |
| $K_M$ | Motor Constant | $5{,}20 \times 10^{-3}\ [N\ m/A]$ |
| $c_c$ | Static Friction Coefficient | $1{,}00 \times 10^{-5}\ [Nm]$ |
| $c_v$ | Viscous Friction Coefficient | $2{,}00 \times 10^{-6}\ [Nms/rad]$ |
| $R$ | Internal Resistance | $0{,}6\ [\Omega]$ |
| $P_{el}$ | Maximum Power per Motor | $35\ [W]$ |
| $I_{max}$ | Maximum Current per Motor | $5\ [A]$ |

The set of waypoints defined during the mission planning is described in Table III, where $[X_W\ Y_W\ Z_W]$ is the desired quadrotor position, $R_W$ is the maximum distance from the center of the waypoint from which the quadrotor heading will be $\psi_W$, and $T_W$ is the hover time over the waypoint.

Table III. SET OF WAYPOINTS

| Index | $X_W[m]$ | $Y_W[m]$ | $Z_W[m]$ | $\psi_W[^\circ]$ | $T_W[s]$ | $R_W[m]$ |
|---|---|---|---|---|---|---|
| $WP_1$ | 0 | 0 | 0 | 0 | 1 | 1 |
| $WP_2$ | 0 | 0 | 20 | 5 | 10 | 1 |
| $WP_3$ | 20 | 0 | 20 | -5 | 5 | 1 |
| $WP_4$ | 20 | 20 | 20 | 10 | 5 | 1 |
| $WP_5$ | 0 | 20 | 20 | -10 | 5 | 1 |
| $WP_6$ | 0 | 0 | 20 | 0 | 10 | 1 |
| $WP_7$ | 0 | 0 | 0 | 0 | 2 | 2 |

The first scenario that the OS4 was submitted consider at $t = 10.0s$ an increase of $10\%$ on the viscous friction of the Motor 1, due to missing lubrication and beginning corrosion. Figures 6 and 7 present the results of path following with fault injection, where the solid lines are the quadrotor's outputs and the dashed line are the desired trajectory.

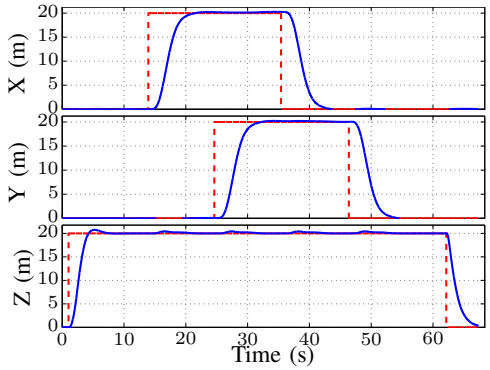


Fig. 6. Quadrotor displacement with fault injection to Motor 1

Comparing these faulty results with those for the nominal fault-free operation, one can observe a negligible difference between both path following performances. Specifically for the attitude tracking, Figure 8 shows a comparison between the performances, where the signals $\phi_D = \phi_N - \phi$, $\theta_D = \theta_N - \theta$ and $\psi_D = \psi_N - \psi$ are the differences between the fault and nominal fault-free operation (expressed by the subscript $N$).

Therefore, this viscous friction in the dynamic system was compensated within a state feedback Multi-Model Predictive

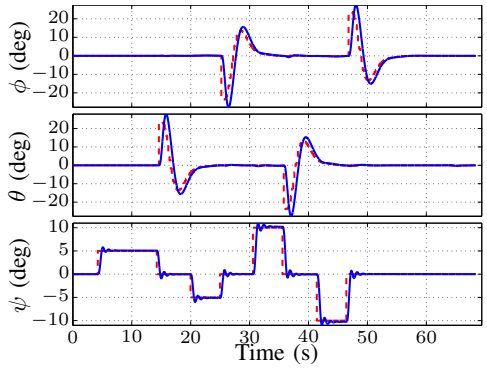


Fig. 7. Attitude path following simulation with fault injection to Motor 1

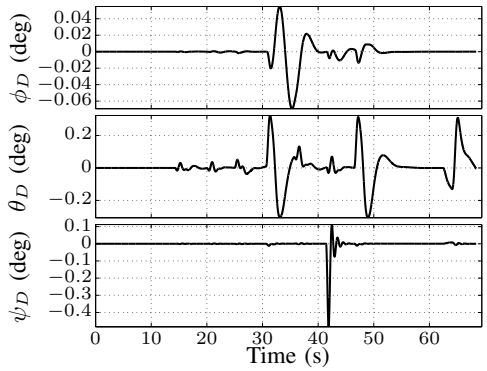


Fig. 8. Negligible difference between the fault-free condition and the attitude signals when the viscous friction of the Motor 1 is increased

Control scheme. However, this fault leads to an increase in the current through the Motor 1, as depicted in Figure 9.

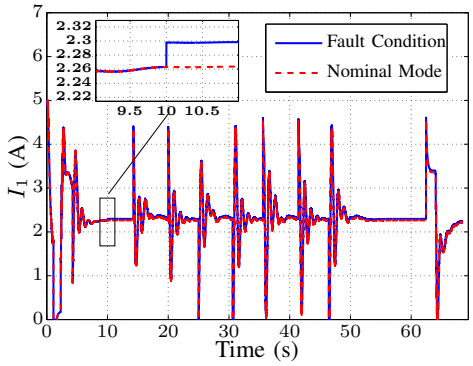


Fig. 9. Current through the motor 1 when at $10.0s$ the viscous friction is increased by $10\%$ (fault condition) and for the nominal mode (without fault)

Although the degree of robustness of the controller is important, it is equally important to ensure reliable fault detection for system and mission dependability. In order to show the performance of the Fault Detection and Diagnosis (FDD), the Interacting Multiple Model (IMM) filter was evaluated for each motor and the results related to the fault detection signals are shown in Figure 10, first when a fixed threshold of $\mu_T = 0.5$ is used (method proposed by [6], according Eq. (8)). The number 1 at "Fault Indicator" axes in Figure 10 is used to suggest a possible fault in the related motor.

According to Figure 10, it is possible to observe the poor performance of the fault detection with this universal threshold. However, if the index $S_j$ proposed in equation (11) is used,

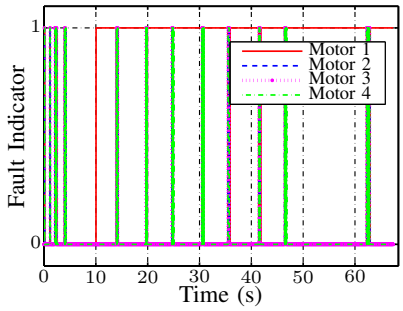


Fig. 10. Fault detection signals when at $10.0s$ the viscous friction of the Motor 1 is increased by $10\%$, using the universal threshold

there is a significant reduction in the number of false alarms, as depicted in Figure 11.

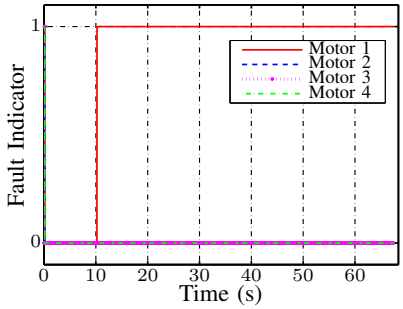


Fig. 11. Fault detection signals when at $10.0s$ the viscous friction of the Motor 1 is increased by $10\%$, using the index $S_j$

The second scenario simulated consider at $t = 10.0s$ an increase of $10\%$ in the phase resistance of all coils of Motor 1, which refers to a rise in stator temperature. One can recognize by Figure 12, that the algorithm detects this fault after $1.2$ second. Again, it is possible to show that the influence of this introduced fault on the MMPC performance can be negligible; all the linear and angular velocities are stabilized and there are no steady-state errors in the positions and orientations.

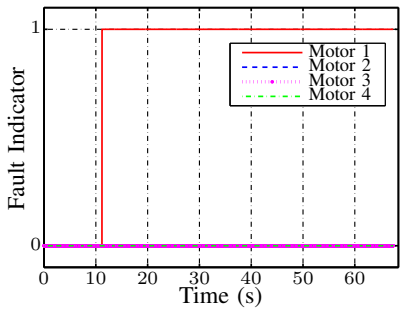


Fig. 12. Fault detection signals when at $10.0s$ the coils' resistance of the Motor 1 is increased by $10\%$, using the index $S_j$

## VI. Conclusion

This paper presented an algorithm for fault detection and diagnosis in brushless dc motors of a quadrotor helicopter, measuring only few accessible signals. The overall performance of the proposed approach was numerically evaluated by simulations, based on the OS4 quadrotor model flying under realistic and fault scenarios, controlled by a Multi-Model Switching Predictive Controller. A new performance index was proposed in order to reduce the false alarms, even in the presence of transient dynamics or small changes in the values of the plant parameters. Future studies could be concerned with real-time implementation aspects for possible deployment in a real quadrotor. In particular, an evaluation of the required computational effort should be carried out.

## Acknowledgment

The authors would like to thank the financial support from Brazilian Agencies FAPESP (Grant 2011/17610-0) and CNPq (Research Fellowships).

## References

[1] S. Bouabdallah, "Design and control of quadrotors with application to autonomous flying," Ph.D. dissertation, École Polytechnique Fédérale de Lausanne, February 2007.

[2] X. Qi, D. Theilliol, J. Qi, Y. Zhang, and J. Han, "A literature review on fault diagnosis methods for manned and unmanned helicopters," in *International Conference on Unmanned Aircraft Systems (ICUAS)*, May 2013, pp. 1114–1118.

[3] A. Freddi, S. Longhi, and A. Monteriu, "Actuator fault detection system for a mini-quadrotor," in *IEEE International Symposium on Industrial Electronics (ISIE)*, July 2010, pp. 2055–2060.

[4] A. Sanchez, L. García Carrillo, E. Rondon, R. Lozano, and O. Garcia, "Hovering flight improvement of a quad-rotor mini uav using brushless dc motors," *Journal of Intelligent & Robotic Systems*, vol. 61, no. 1-4, pp. 85–101, 2011.

[5] I. González, S. Salazar, J. Torres, R. Lozano, and H. Romero, "Real-time attitude stabilization of a mini-uav quad-rotor using motor speed feedback," *Journal of Intelligent & Robotic Systems*, vol. 70, no. 1-4, pp. 93–106, April 2013.

[6] Y. Zhang and X. Rong Li, "Detection and diagnosis of sensor and actuator failures using imm estimator," *IEEE Transactions on Aerospace and Electronic Systems*, vol. 34, no. 4, pp. 1293–1313, Oct 1998.

[7] H. A. Izadi, Y. Zhang, and B. W. Gordon, "Fault tolerant model predictive control of quad-rotor helicopters with actuator fault estimation," in *Proceedings of the 18th IFAC World Congress*, August 2011, pp. 6343–6348.

[8] K. Alexis, G. Nikolakopoulos, and A. Tzes, "Switching model predictive attitude control for a quadrotor helicopter subject to atmospheric disturbances," *Control Engineering Practice*, vol. 19, no. 10, pp. 1195 – 1207, 2011.

[9] O. Moseler and R. Isermann, "Application of model-based fault detection to a brushless dc motor," *IEEE Transactions on Industrial Electronics*, vol. 47, no. 5, pp. 1015–1020, 2000.

[10] E. F. Camacho and C. Bordons, *Model Predictive Control*. Springer, August 1999.

[11] S. Qin and T. A. Badgwell, "A survey of industrial model predictive control technology," *Control Engineering Practice*, vol. 11, no. 7, pp. 733 – 764, July 2003.

[12] L. Giovanini, A. Ordys, and M. Grimble, "Adaptive predictive control using multiple models, switching and tuning," *International Journal of Control, Automation and Systems*, vol. 4, no. 6, pp. 669–681, November 2006.

[13] H. Chen, L. Ning, and L. Shaoyuan, "Switching multi-model predictive control for hypersonic vehicle," in *8th Asian Control Conference (ASCC)*, May 2011, pp. 677–681.

[14] A. S. Cândido, R. K. H. Galvão, and T. Yoneyama, "Comparative assessment of predictive controllers for an inverted pendulum with three conflicting control objectives," in *20th International Congress of Mechanical Engineering (COBEM)*. Gramado, Brazil: ABCM, 2009.

[15] F. Sharifi, M. Mirzaei, B. Gordon, and Y. Zhang, "Fault tolerant control of a quadrotor uav using sliding mode control," in *Conference on Control and Fault-Tolerant Systems (SysTol)*, Oct 2010, pp. 239–244.

[16] S. Julier and J. Uhlmann, "Unscented filtering and nonlinear estimation," *Proceedings of the IEEE*, vol. 92, no. 3, pp. 401–422, 2004.